

Rarefaction acceleration of ultrarelativistic magnetized jets in gamma-ray burst sources

Serguei S. Komissarov,^{1*} Nektarios Vlahakis^{2*} and ArieH Königl^{3*}

¹*Department of Applied Mathematics, The University of Leeds, Leeds, LS2 9GT*

²*Section of Astrophysics, Astronomy and Mechanics, Physics Department, University of Athens, 15784 Zografos, Athens, Greece*

³*Department of Astronomy and Astrophysics and Enrico Fermi Institute, University of Chicago, 5640 South Ellis Avenue, Chicago, IL 60637, USA*

Received/Accepted

ABSTRACT

When a magnetically-dominated super-fast magnetosonic GRB jet leaves the progenitor star the external pressure support may drop and the jet may enter the regime of ballistic expansion during which its magnetic acceleration becomes highly ineffective. However, recent numerical simulations suggested that the transition to this regime is accompanied by a sudden “burst” of acceleration. We confirm this finding and attribute the acceleration to the sideways expansion of the jet - the magnetic energy is converted into the kinetic one in the strong magnetosonic rarefaction wave, which is launched when the jet loses its external support. This type of acceleration, *the rarefaction acceleration*, is specific to relativistic jets because their energy budget can still be dominated by magnetic energy even in highly super-fast magnetosonic regime. Just like the *collimation acceleration* of externally confined magnetized jets, it is connected with the geometry of magnetic flux surfaces. In both cases, in the acceleration zone the poloidal field lines diverge faster than in the monopolar configuration. On the other hand, whereas the collimation acceleration keeps the product of jet opening angle and Lorentz factor somewhat below unity, the rarefaction acceleration allows to make it significantly larger, in agreement with the standard model of jet breaks in afterglow light curves.

Key words: MHD – relativity – methods: numerical – gamma-rays: bursts

1 INTRODUCTION

In the “standard” model of long-duration, soft-spectrum gamma-ray bursts (GRBs; e.g. Piran 2005), the prompt high-energy emission arises in ultra-relativistic (bulk Lorentz factor $\Gamma \gtrsim 10^2$), highly collimated (opening half-angle of a few degrees) jets. The high Lorentz factors are inferred from the requirement of a sufficiently low opacity to photon-photon annihilation or to scattering by photon annihilation-produced electron-positron pairs (e.g. Lithwick & Sari 2001). The high collimation allows to reduce the total flow energy down to the values comparable with the energy of stellar explosions.

As the jets make their way through the interstellar medium they sweep the interstellar gas into a thin relativistic shell which itself becomes a strong source of electromagnetic radiation. Once the mass of the swept gas becomes

significant the shell begins to decelerate and the simplified models of this interaction predict a panchromatic break in the afterglow light curve, provided that $\Gamma\theta_j \gg 1$, where θ_j is the jet half-opening angle. The detections of such “jet breaks” in some of the early afterglow observations is the main reason why the jet model of GRBs is so popular today. The observed break parameters have allowed to deduce the jet opening half-angle, usually in the range of $1^\circ - 10^\circ$ (e.g. Rhoads 1999; Sari et al. 1999). This result, however, is strongly model-dependent. Although, the more recent observations by the *Swift* satellite have revealed that the jet breaks are not that common and that various aspects of the jet model may need to be modified (e.g. Mészáros 2006; Panaitescu 2007; Liang et al. 2008), the breaks remain the strongest evidence for the collimated outflow so far.

The supernova connection of long GRBs provides strong support for the theoretical models of their jet engines that invoke dying massive and rapidly rotating stars. These models are generally divided into two groups depending on the mechanism of jet acceleration. In the first group the accel-

* E-Mail: serguei@maths.leeds.ac.uk (SSK); vlahakis@phys.uoa.gr (NV); arieh@jets.uchicago.edu (AK)

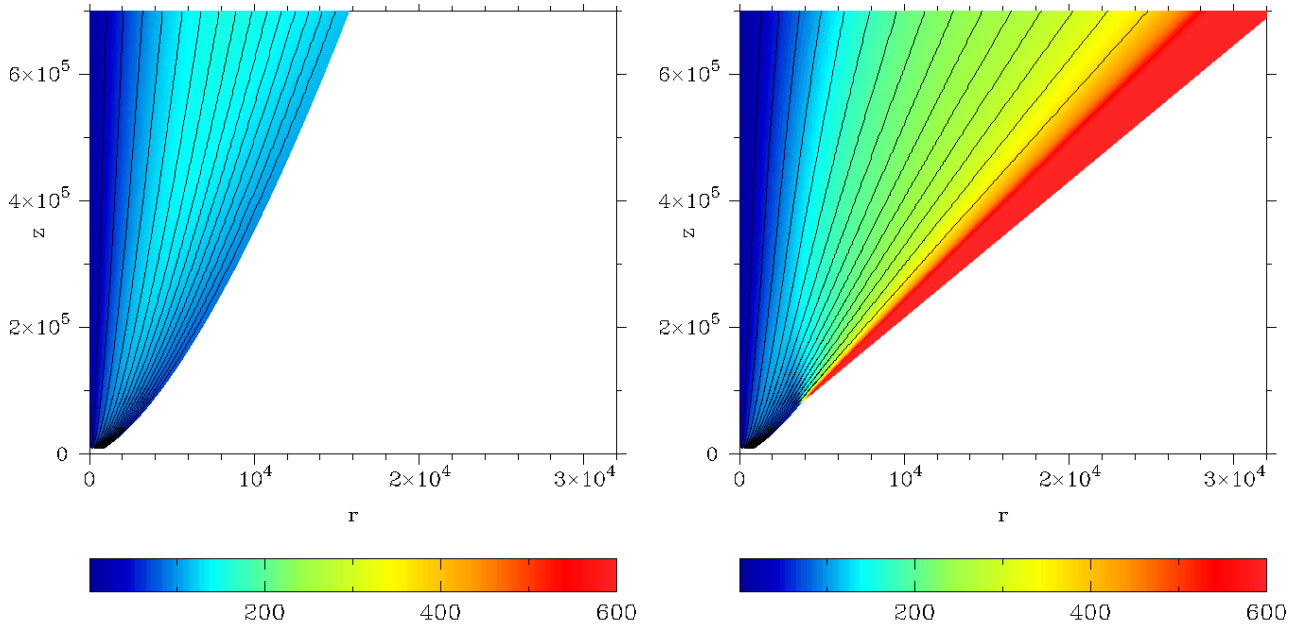


Figure 1. Lorentz factor and magnetic field lines in models B1 (left panel) and B1b (right panel).

eration is driven by the thermodynamic pressure of plasma heated to ultra-relativistic temperatures via the annihilation of neutrinos and antineutrinos emitted by the accretion disk formed around the central black hole, thus tapping the disk thermal energy. In the second group the acceleration is driven by the magnetic stresses, tapping the rotational energy of the disk or the central compact object, neutron star or black hole. At present, both the magnetic and the thermal mechanisms seem possible, although the lack of detection of a thermal component in the spectra of some GRBs is in favour of initially magnetically dominated outflows (Zhang & Pe'er 2009).

The potential of magnetic mechanism has been a subject of theoretical study for many years. Due to the mathematical complexity of magnetohydrodynamics (MHD), further amplified in the relativistic limit, it has been possible to find analytical and semi-analytical solutions only for a rather limited number of problems characterised by a high degree of symmetry. In fact, there is only one available *exact* solution of the relativistic MHD equations including thermal and magnetic effects, the self-similar model of Vlahakis & Königl (2003). The advance of numerical methods for relativistic MHD during the last decade has opened a new direction of study which has already proved to be very helpful (e.g. Komissarov 2001, 2004; McKinney 2006; Komissarov & Barkov 2007; Komissarov et al. 2007; Tchekhovskoy et al. 2008; Bucciantini et al. 2008; Komissarov et al. 2009; Tchekhovskoy et al. 2009a; Komissarov & Barkov 2009; Tchekhovskoy et al. 2009b; McKinney & Blandford 2009; Bucciantini et al. 2009).

In particular, Komissarov et al. (2009) investigated the magnetic acceleration of ultra-relativistic flow within channels of prescribed geometry, $z \propto r^a$, determined by the shape of coordinate surfaces of elliptical coordinates. Such shapes correspond to the power law pressure distribution of confining medium, which can approximate the collapsing star in

both the collapsar and magnetar scenarios, as well as the disk wind. Among other results, they have found that in the case of gradually opening channel, $a < 1$, the acceleration is not efficient, whereas in the case of a channel with gradually increasing collimation, $a > 1$, the acceleration is effective but the asymptotic flows satisfy the condition $\Gamma\theta_j \leq 1$. These numerical results have been strengthened by complimentary theoretical analysis (Komissarov et al. 2009; Lyubarsky 2009) and raised the question of whether the magnetic models can accommodate the jet breaks at all. Recently, a similar numerical study has been carried out by Tchekhovskoy et al. (2009b) which has confirmed the findings of Komissarov et al. (2009). Moreover, they have also considered a somewhat modified setup, where at some distance from the origin, roughly corresponding to the stellar surface, the channel geometry changes from progressively collimated to progressively de-collimated. In this setup they observed a remarkable change in the jet behaviour after the point of transition, characterised by a strong boost in the jet speed accompanied by only a very small increase in the jet opening angle. As a result, the asymptotic flow has $\Gamma\theta_j \gg 1$, now allowing the possibility of jet breaks. The exact shape of the channel above the transition point did not seem to matter.

In this paper we describe the simulations which confirm the results of Tchekhovskoy et al. (2009b) and analyse the underlying physical mechanism.

2 NUMERICAL SIMULATIONS

The numerical method is exactly the same as in Komissarov et al. (2009) and we refer the reader interested in technical details to this paper. Here we only remark that our numerical code is based on the Godunov-type scheme for relativistic MHD (Komissarov 1999) and that we look for

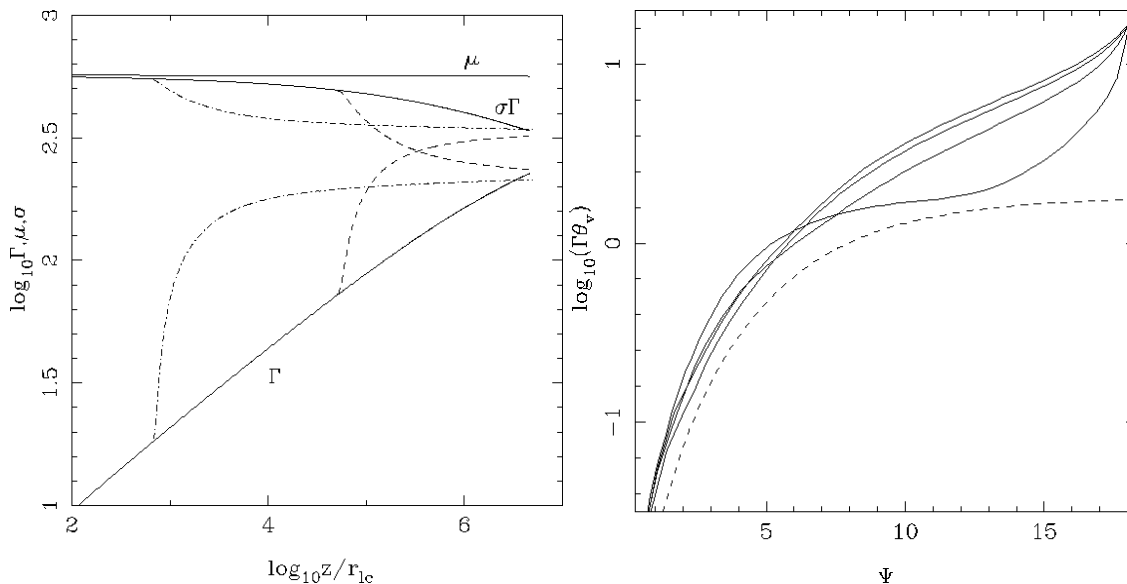


Figure 2. Left panel: Evolution of Γ , $\sigma\Gamma = \mu - \Gamma$, and μ along the magnetic surface enclosing 80% of the total magnetic flux ($\Phi = 15$) in models B1 (solid line), B1a (dash-dotted line), and B1b (dashed line). Right panel: Evolution of $\Gamma\theta_v$ along the jet in model B1b. The solid lines show the variation of this parameter as a function of magnetic flux (Ψ) inside the jet cross sections located at $z = 1, 2, 4$ and 8×10^5 , higher value of z corresponding to higher curve at $\Psi = 15$. The dashed curve shows $\Gamma\theta_v$ at $z = 8 \times 10^5$ in model B1.

steady-state axisymmetric solutions using time-dependent simulations with time-independent boundary conditions.

For our purpose we selected model B1 from Komissarov et al. (2009) where the channel shape parameter $a = 3/2$. This model describes cold flow with energy flux per unit rest mass flux up to $\mu = 620$ – this value gives the highest possible asymptotic value of the Lorentz factor, corresponding to complete conversion of Poynting flux into the kinetic energy. The initial ratio of the Poynting flux to the hydrodynamic energy flux $\sigma_0 = \mu/\Gamma_0 - 1 \simeq \mu$, as the initial Lorentz factor, Γ_0 , is close to unity, corresponding to sub-Alfvénic flow. The base rotation is uniform with the dimensionless light cylinder radius $r_{1c} \simeq 1.6$; we used the distance of the inlet boundary from the origin to setup the unit length.

To see the effect of changing the channel shape we mapped the solution at $z \simeq 10^3$ and 7×10^5 onto the inlet boundary of new grid corresponding to the conical channel of the same local radius and the vertex located at the origin. This way we introduce a break in the channel shape leading to a lower collimation. Then we proceed with the simulations on the new grid following the same procedure as in model B1. The resultant solutions, which we denoted as B1a and B1b, are analysed below.

Fig. 1 shows the overall geometry of both models B1 and B1b, including the shape of magnetic surfaces, and the evolution of the Lorentz factor in both models. One can see that in contrast to model B1 the field lines in model B1b straighten up. One might think this reflects the conical shape of its channel but this is not so. In fact, the jet is separated from the channel wall by almost vacuum¹. This is the reason why the red-coloured boundary layer in the right panel of Fig. 1 is free from magnetic field lines. A similar separation

has been seen in model E in Komissarov et al. (2009) and, we believe, in the simulations by Tchekhovskoy et al. (2009b). As a result, the wall and the jet are causally disconnected and the precise shape of the wall does not matter.

In model B1b the jet Lorentz factor approaches its maximum possible value $\Gamma_{\max} = \mu$ at the jet boundary, signalling total conversion of the Poynting flux. The acceleration is weaker in the jet interior but, as one can see clearly in Fig. 1, it is still more effective than in model B1. This is further illustrated in the left panel of Fig. 2, which compares the acceleration in both models along the magnetic surface enclosing 80% of the jet’s total poloidal magnetic flux. As to the model B1a, where the channel opens up much earlier, the jet also passes through the phase of rapid acceleration. However, the acceleration then slows down dramatically as the jet enters the phase of ballistic expansion. As a result, the final Lorentz factor in this model is even slightly lower compared to model B1. As one can see from Fig. 1 the opening of the jet does not change much after passing the channel opening point, in agreement with the results by Tchekhovskoy et al. (2009b). Thus, the product $\Gamma\theta_v$, where θ_v is the half-opening angle, is expected to increase following the rapid increase of the Lorentz factor. This is indeed the case, as one can see in the right panel of Fig. 2. In model B1b this parameter is much higher than in model B1, approaching values $\Gamma\theta_v \gg 1$ near the jet boundary. Concluding this section, we state that our results are in very good agreement with those obtained in Tchekhovskoy et al. (2009b), thus confirming that the effect is real and must have a robust physical nature.

3 ACCELERATION MECHANISM

Once the jet separates from the wall it enters the phase of free expansion and eventually becomes a ballistic conical outflow with radial streamlines. During the transition from

¹ In the simulations the mass density in the vacuum zone is kept above zero due to a number of numerical factors.

one regime to another a strong rarefaction wave travels inside the jet and the observed acceleration has to be related to the properties of this wave. In fact, this phenomenon has already been established both in the magnetic and in the pure gasdynamic regimes (Aloy & Rezzolla 2006; Mizuno et al. 2008). Here we elucidate its physical nature.

Consider a simple one dimensional problem with plane geometry describing the evolution of initial discontinuity that separates uniform magnetized cold plasma at rest on the left and vacuum on the right. This problem is obviously related to the transverse expansion of our simulated jets after they lose the external support, as seen in the jet co-moving frame. The discontinuity decays into a single wave, namely the fast magnetosonic rarefaction wave. The left front of this wave propagates into the left state with the local fast magnetosonic speed and the right front moves into vacuum with some finite terminal speed. In such a simple geometry, the Lorentz force reduces to the magnetic pressure and the equations of MHD reduce to those of hydrodynamics of ideal gas with the ratio of specific heats $\gamma = 2$, the effective sound speed being equal to the fast magnetosonic speed,

$$a = c_f = c \frac{b}{\sqrt{4\pi\rho c^2 + b^2}}, \quad (1)$$

where b is the strength of magnetic field in the comoving frame. This property allows us to use the results obtained in relativistic gasdynamics, in particular its Riemann invariants (Martí & Müller 1994). This way we find that

$$J_+ = \left(\frac{1 + v_0/c}{1 - v_0/c} \right) \left(\frac{1 + c_f/c}{1 - c_f/c} \right)^2, \quad (2)$$

where v_0 is the local flow speed, is constant across the rarefaction. This equation suggests a simple way of finding the speed of expansion in vacuum. On one hand, given the left state we can compute J_+ . On the other hand, at the boundary with vacuum $c_f = 0$ and thus

$$v_0 = \frac{J_+ - 1}{J_+ + 1} c. \quad (3)$$

For example, if in the left state, where $v_0 = 0$, we have $b^2 = 4\pi\rho c^2$, and hence $c_f = c/\sqrt{2}$ then the Lorentz factor of expansion in vacuum is $\Gamma_0 = 3$.

Next consider another frame that moves along the initial discontinuity with Lorentz factor Γ – this corresponds to the jet source frame in our simulations. The Lorentz factor of plasma at the right front of the rarefaction wave in this frame is

$$\Gamma_1 = \Gamma\Gamma_0, \quad (4)$$

which is three times higher than Γ . Thus, the seemingly weak acceleration in the initial fluid frame may correspond to a huge boost in the moving frame – for the example considered earlier the Lorentz factor increases from $\Gamma = 200$ to the left of the rarefaction wave to $\Gamma_1 = 600$ at the boundary with vacuum. This is the essence of the acceleration during the transition to the free expansion regime that is observed in our jet simulations.² The speed of expansion in vacuum in

² In fact, the situation is a little bit more complicated as explained in Appendix A.

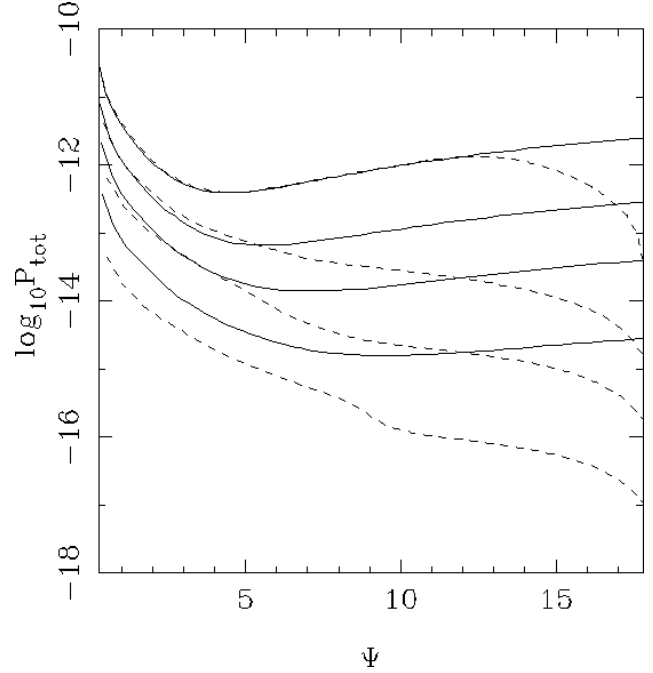


Figure 3. Propagation of rarefaction wave across the jet in model B1b. The solid lines show the magnetic pressure distribution in the cross-sections at $z = 1, 3, 9, 30 \times 10^5 r_{1c}$ for model B1, the dashed lines show the corresponding distributions for model B1b (higher is the value of z , lower is the curve.)

this frame is v_0/Γ . For our jet problem this implies that (i) the jet opening angle cannot increase by more than $1/\Gamma$, in agreement with the results of our simulations, and (ii) the product $\Gamma\theta_v$ increases to values significantly larger than unity mainly due to the increase of Γ .

In model B1 the jet is causally connected (see Komissarov et al. 2009), that is a fast magnetosonic wave emitted at the boundary can reach the jet axis. Therefore, the fast magnetosonic rarefaction wave originated from the opening of the channel in models B1a and B1b is not confined to a boundary layer but propagates all the way to the jet core and causes acceleration throughout the whole of jet volume. This is clearly seen in Fig. 3 which compares the distributions of magnetic pressure, $b^2/8\pi$, in models B1 and B1b downstream of the opening.

The above interpretation agrees with the general analysis of the acceleration of cold steady-state jets in Komissarov et al. (2009), where it is shown that the bulk flow acceleration is inseparably connected with the shape of the field-streamlines, through the “bunching function”

$$S = \frac{\pi r^2 B_p}{\Psi}, \quad (5)$$

where r is the cylindrical distance from the rotation axis, B_p is the strength of poloidal magnetic field, and $\Psi = \int \mathbf{B}_p \cdot d\mathbf{S}$ is the magnetic flux function. Namely, in the super-fast magnetosonic regime the Lorentz factor increases when S decreases. In fact, one can show that

$$\left(\frac{v^2}{c^2} - \frac{\mu - \Gamma}{\Gamma^3} \right) \frac{d(\Gamma v)}{d\ell} = -\frac{2}{mc} \frac{dS}{d\ell} \quad (6)$$

where ℓ is the distance measured along the poloidal mag-

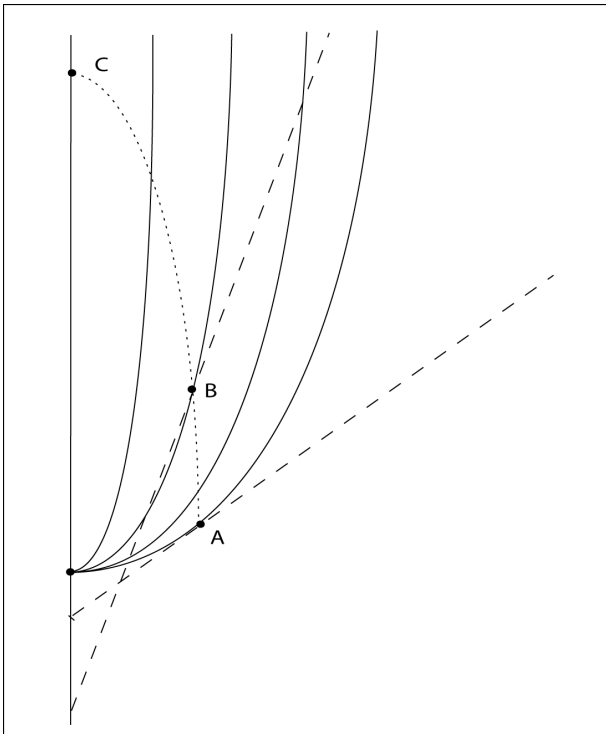


Figure 4. Straightening of the jet magnetic field lines after the channel opening. In this sketch the solid lines show the magnetic field of an externally confined jet, the dashed lines show the radial magnetic field lines of a ballistic jet, and the dotted line shows the location of the rarefaction wave front. The magnetic field lines of the jet that becomes free after passing a sudden opening of the confining channel (point A) are represented by the solid lines upstream of the rarefaction front and by the dashed lines downstream of it (for simplicity we assume that the field lines straighten up right after crossing the front). The figure shows two such field lines, crossing the rarefaction fronts at points A and B respectively. As we move along the jet from A to B the inner line is still parabolic whereas the outer one is already straight. Thus, the separation between them increases faster than r and the magnetic field strength decreases faster than r^{-2} .

netic field lines and m is constant on magnetic flux surfaces (see Appendix B). The coefficient in front of the derivative on the left hand side of this equation vanishes at the fast magnetosonic critical surface (in the relativistic cases this gives $\Gamma \approx \mu^{1/3}$). Thus, in the super-fast magnetosonic regime acceleration corresponds to decreasing \mathcal{S} , whereas in the sub-fast magnetosonic regime it corresponds to increasing \mathcal{S} . This is analogous to the transonic hydrodynamic flow in the De Laval nozzle, with $1/\mathcal{S}$ playing the role of the nozzle's cross-section.

Equation (5) shows that for \mathcal{S} to decrease B_p should decrease faster than r^{-2} , and thus the separation between magnetic field lines should increase with distance faster than in the monopolar configuration. In confined flows, such as B1 and others studied in Komissarov et al. (2009), this is realised via the stronger collimation of the inner flux surfaces in relation to the outer ones. For this reason, the acceleration mechanism at work in such flows can be called the *collimation mechanism*.

In the *rarefaction mechanism*, that operates in models B1a and B1b during the transition to ballistic regime, the

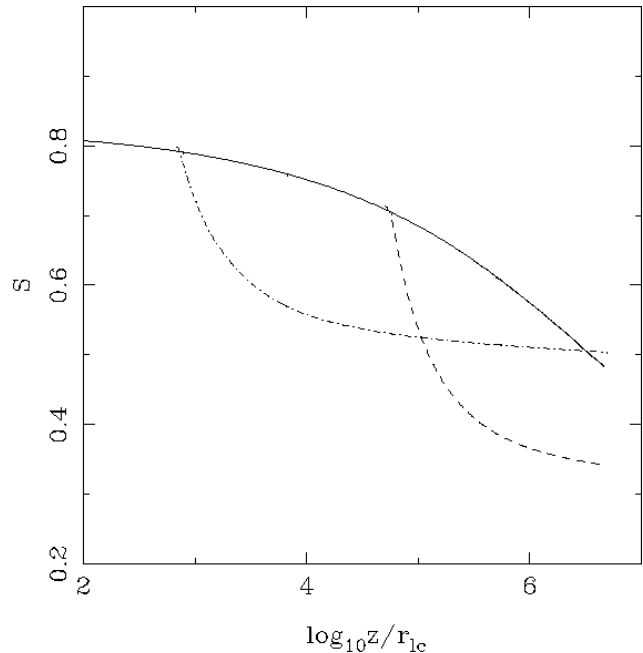


Figure 5. Evolution of the bunch function, \mathcal{S} along the magnetic surface with $\Phi = 15$ for models B1 (solid line), B1a (dash-dotted line), and B1b (dashed line).

rarefaction wave reaches the jet axis much further downstream of the channel opening and, thus, the outer field lines straighten up much closer to the source compared to the inner ones (see Fig. 4). The net effect is still B_p decreasing faster than r^{-2} . Inspection of models B1a and B1b shows that the magnetic bunching function is indeed decreasing along the magnetic field lines (see Fig. 5) and that in both these models the flow becomes super fast-magnetosonic well upstream of the channel opening point.³

4 DISCUSSION AND CONCLUSIONS

Our numerical simulations confirm the discovery by Tchekhovskoy et al. (2009b) of the additional fast acceleration of relativistic jets during the transition from confined to unconfined regime. We have also analyzed the mechanism of the acceleration and concluded that it is related to the sideways expansion of the jet triggered by the disappearance of the support from the confining wall. This expansion does not lead to a significant increase of the jet opening angle because of the very high Mach number of the jet at the point of the channel opening. In spite of this the rarefaction wave is strong and allows to convert a large fraction of the magnetic energy into the kinetic energy of bulk motion.

This mechanism and its potential application to relativistic astrophysical flows has been already discussed by Aloy & Rezzolla (2006) and Mizuno et al. (2008). Although, it operates even in Newtonian flows its role there is not that important. For Newtonian flows, high fast magnetosonic

³ The sub-fast magnetosonic regime is realised in model E of Komissarov et al. (2009) where it was found that an early opening of the jet boundary does not accelerate the flow.

Mach number implies that most of the magnetic energy has already been converted into the bulk motion kinetic energy and any additional acceleration would be rather insignificant even if it involved full conversion of magnetic energy. In the relativistic case this is not true anymore as flows can remain magnetically dominated even in the highly super-fast magnetosonic regime.

We have shown that when the rarefaction wave propagates inside the jet it produces a region where the separation between poloidal magnetic field lines increases faster than in the monopolar configuration. In fact, this is a common feature of magnetic acceleration in super-fast magnetosonic regime – it is also characteristic for the magnetic acceleration of externally confined flows via the *collimation mechanism*. However, there are also significant differences between these mechanisms. Most importantly, the acceleration via the *collimation mechanism* can be sustained over many decades in the distance and produces asymptotic flows with $\sigma \simeq 1$, whereas the *rarefaction mechanism* continues only for as long as it takes for the rarefaction wave to cross the jet (\simeq jet length in our numerical models). After this the flow enters the phase of ballistic expansion where the magnetic acceleration is so slow that it can be ignored.

The most effective magnetic acceleration of steady flows can be achieved via a combination of both mechanisms – first the collimation mechanism produces a flow with $\sigma \simeq 1$, and then the rarefaction mechanism provides additional acceleration, resulting in a particle dominated flow. Model B1b is a close example of such combination (see Fig. 2). Let us see if this is achievable in the context of long GRBs. If the jet originates from a rapidly rotating black hole (BH) then the light cylinder radius is of order of few gravitational radii, $r_{lc} \simeq 2 \times 10^6$ cm for a three solar mass BH. If the confining medium is the stellar envelope, the collimation mechanism operates up to $10^3 r_{lc}$. Quick inspection of Fig. 2 shows that this corresponds to the channel opening point in our model B1b. Thus, it is indeed possible to achieve flows with very high Lorentz factor, as required by observations, and $\sigma \leq 1$ at $r \simeq 10^{12}$ cm. If, however, the initial magnetization is very high, well above $\sigma_0 \simeq 10^3$, the jet will still remain magnetically dominated when it enters the ballistic regime (as it is assumed in the magnetodynamic model of GRB jets by Lyutikov & Blandford 2003).

Another important property of the rarefaction mechanism in the context of GRB studies, as has been pointed out by Tchekhovskoy et al. (2009b), is the possibility to produce flows with $\Gamma\theta_j \gg 1$. In the standard model of uniform GRB jet this condition allows jet breaks in the light curves of afterglow emission. However the asymptotic structure of magnetically accelerated jets is far from being uniform and further investigation is required in order to clarify this issue.

ACKNOWLEDGMENTS

SSK was supported by the STFC rolling grant “Theoretical Astrophysics in Leeds”. NV acknowledges partial support by the Special Account for Research Grants of the National and Kapodistrian University of Athens. AK was partially supported by a NASA Astrophysics Theory Program grant.

REFERENCES

- Aloy M. A., Rezzolla L., 2006, ApJ, 640, L115
 Barkov M. V., Komissarov S. S., 2008, MNRAS, 385, L28
 Bucciantini N., Quataert E., Arons J., Metzger B. D., Thompson T. A., 2008, MNRAS, 383, L25
 Bucciantini N., Quataert E., Arons J., Metzger B. D., Thompson T. A., Arons J., Del Zanna L., 2009, MNRAS, 396, 2038
 Daigne F., Drenkhahn G., 2002, A&A, 381, 1066
 Komissarov S. S., 1999, MNRAS, 303, 343
 Komissarov S. S., 2001, MNRAS, 326, L41
 Komissarov S. S., 2004, MNRAS, 350, 1431
 Komissarov S. S., Barkov M. V., 2007, MNRAS, 382, 1089
 Komissarov S. S., Barkov M. V., 2009, MNRAS, 397, 1153
 Komissarov S. S., Barkov M. V., Vlahakis N., Königl A., 2007, MNRAS, 380, 51
 Komissarov S. S., Vlahakis N., Königl A., Barkov M. V., 2009, MNRAS, 394, 1182
 Liang E.-W., Racusin J. L., Zhang B., Zhang B.-B., Burrows D. N., 2008, ApJ, 675, 528
 Lithwick Y., Sari, R., 2001, ApJ, 555, 540
 Lyubarsky Yu., 2009, ApJ, 698, 1570
 Lyutikov M., Blandford R.D., 2003, astro-ph.12347
 Martí J.M., Müller E., 1994, J.Fluid Mech., 258, 317
 McKinney J. C., 2006, MNRAS, 368, 1561
 McKinney J. C., Blandford R. D., 2009, MNRAS, 394, L126
 Mészáros P., 2006, Rep. Prog. Phys., 69, 2259
 Mizuno Y., Hardee P., Hartmann D. H., Nishikawa K.-I., Zhang B., 2008, ApJ, 672, 82
 Panaitescu A., 2007, MNRAS, 379, 331
 Piran T., 2005, Rev. Mod. Phys., 76, 1143
 Rhoads J. E., 1999, ApJ, 525, 737
 Sari R., Piran T., Halpern J. P., 1999, ApJ, 519, L17
 Tchekhovskoy A., Narayan R., McKinney J. C., 2008, MNRAS, 388, 551
 Tchekhovskoy A., Narayan R., McKinney J. C., 2009a, ApJ, 699, 1789
 Tchekhovskoy A., Narayan R., McKinney J. C., 2009b, arXiv0909.0011
 Vlahakis N., 2004, ApJ, 600, 324
 Vlahakis N., Königl A., 2003, ApJ, 596, 1080
 Zhang, B. and Pe’er, A., 2009, ApJ, 700, L65

APPENDIX A: RIEMANN PROBLEMS WITH AND WITHOUT TANGENTIAL VELOCITY

The Riemann problem considered in Sec.3 describes the left state ($x < 0$) with $\mathbf{v} = (0, 0, 0)$, $\mathbf{B} = (0, 0, b)$, $b = \sqrt{4\pi\rho c^2}$, $p = 0$, and the right state ($x > 0$) with $\mathbf{v} = (0, 0, 0)$, $\mathbf{B} = (0, 0, 0)$, $\rho = p = 0$. Its solution describes simple rarefaction wave with the Lorentz factor at the right front $\Gamma_0 = 3$. Let us modify this problem via introduction of tangential motion along the initial discontinuity (without any loss of generality we assume that its velocity is perpendicular to the direction of magnetic field, that is $\mathbf{v} = (0, v, 0)$). Both the magnetic pressure and rest-mass density are kept the same as before. Given the analysis of Section 3, one could naively expect that the Lorentz factor at the right front of the rarefaction wave will be simply given by the Lorentz transformation be $\Gamma_1 = \Gamma\Gamma_0 = 600$ if $\Gamma = 200$. However,

as one can see in Fig. A1, which shows the results of actual integration along the rarefaction, this is not the case – this Lorentz factor is noticeably lower. Another unexpected result is the variation of v_y along the rarefaction – indeed if this component is simply a result of Lorentz boost in the y direction than v_y must be constant. The reason for these differences is simply that these two Riemann problems are not related by the Lorentz boost along the y -axis. In order to see this we notice that the decay of initial discontinuity can be viewed as a result of simultaneous burst of a plane membrane separating two states. However, due to the relativity of simultaneity the simultaneous burst of membrane in one frame will not be simultaneous in another frame which is moving relative to the first one parallel to the membrane. Thus, although the Lorentz boost argument provides nice and simple qualitative explanation of the acceleration observed in our jet simulations, it cannot substitute the actual simulations.

APPENDIX B: BUNCHING FUNCTION AND MAGNETIC ACCELERATION

At distances from the central source where the flow can be considered cold and the azimuthal velocity small, the component of the momentum equation along the motion can be written as

$$\frac{\Gamma\rho}{2} \left(1 + \Gamma^2 \frac{v^2}{c^2} \right) \frac{dv^2}{d\ell} = - \frac{B_\phi}{4\pi r} \frac{d(rB_\phi)}{d\ell}, \quad (\text{B1})$$

where ρ is the rest mass-density, r is the cylindrical coordinate, B_ϕ is the azimuthal component of the magnetic field, ℓ is the arclength along a poloidal field-streamline, and derivatives with respect to ℓ are taken along a given field-streamline (see, e.g., eq.[20] in Vlahakis & Königl 2003).

We can further simplify equation (B1) by using two integrals of motion, the mass flux per unit magnetic flux (k) and the angular velocity of magnetic field lines (Ω) (see, e.g., Section 2.1 in Komissarov et al. 2009). Using their expressions in the limit of small azimuthal velocity

$$k = \frac{\rho\Gamma v}{B_p}, \quad \Omega = - \frac{v}{r} \frac{B_\phi}{B_p}, \quad (\text{B2})$$

equation (B1) can be written in the form of a momentum equation of a point particle in a potential field

$$m \frac{d(\Gamma v)}{dt} = - \frac{d\mathcal{V}}{d\ell}. \quad (\text{B3})$$

The effective rest mass, m , is inversely proportional to the magnetization

$$m = \frac{8\pi^2 kc}{\Psi\Omega^2}, \quad (\text{B4})$$

and the effective potential energy is related to the bunching function

$$\mathcal{V} = \frac{2\mathcal{S}}{v/c}. \quad (\text{B5})$$

The corresponding energy equation can be written

$$m\Gamma c^2 + \mathcal{V} = m\mu c^2, \quad (\text{B6})$$

with the integral μ being equal with the total energy flux per unit rest-mass energy flux.

The bunching function \mathcal{S} is directly connected to the geometry of the flow. The cross section area between two neighbouring field-lines Ψ and $\Psi + \delta\Psi$, is $\delta\Psi/B_p$. Thus, the function \mathcal{S} is proportional to r^2 over this area, and decreases whenever the flow expands in a way such that this area increases faster than r^2 (Vlahakis 2004; see also Section 5.1 in Komissarov et al. 2009). \mathcal{S} can be regarded as the solution of the transfield component of the momentum equation, and is connected to the external pressure of the jet and the shape of the “wall” separating the jet with its environment.

Since the potential depends not only on \mathcal{S} , but the velocity as well, it is better to separate the effect of geometry in the equation of motion. Combining equations (B3), (B5), (B6) we can write

$$\left(\frac{v^2}{c^2} - \frac{\mu - \Gamma}{\Gamma^3} \right) \frac{d(\Gamma v)}{d\ell} = - \frac{2}{mc} \frac{d\mathcal{S}}{d\ell}. \quad (\text{B7})$$

The resulting critical point corresponds to the fast magnetosonic surface, where $d\mathcal{S}/d\ell = 0$ and $\Gamma \approx \mu^{1/3}$ (in the relativistic cases where $1 \ll \Gamma \ll \Gamma^3$). Acceleration in the superfast (sub-fast) magnetosonic regime corresponds to decreasing (increasing) \mathcal{S} , respectively.

If at some point the curvature of the jet boundary suddenly increases, the adjustment of the magnetic field from the old to the new curvature corresponds to a fast expansion and decrease of the bunching function. This is precisely the result of the *rarefaction* wave analysed in Section 3. As an example, suppose that the initial shape is parabolic $z = c_1 r^{c_2}$ and the final conical $z = z_0 + r/\tan\vartheta_{\text{tr}}$, as shown in Fig. 4. The z_0 and ϑ_{tr} are functions of Ψ , and can be found from the smooth matching of the magnetic field along a surface $z_{\text{tr}} = z_{\text{tr}}(r_{\text{tr}})$ (dotted line in Fig. 4). Downstream from this transition surface the bunching function \mathcal{S} declines as

$$\mathcal{S} = \frac{\mathcal{S}_{\text{tr}} + \Delta\mathcal{S}}{1 + \frac{\Delta\mathcal{S}}{\mathcal{S}_{\text{tr}}} \frac{r_{\text{tr}}}{r}}, \quad \Delta\mathcal{S} = -\mathcal{S}_{\text{tr}} \frac{\sin^2\vartheta_{\text{tr}}}{r_{\text{tr}}} \frac{dz_0}{d\vartheta_{\text{tr}}} \quad (\text{B8})$$

(for details, see eq. [35] and related discussion in Vlahakis 2004). The appearance of the $z_0(\Psi)$ in the equation of the conical shape $z = z_0 + r/\tan\vartheta_{\text{tr}}$ is crucial, and allows for the additional acceleration ($\Delta\mathcal{S} < 0$). See the related discussion on the difference between “type I conical” (in which $z_0 = 0$) and “type Ia conical” shapes, in Vlahakis (2004); similar categories exist in parabolic shapes as well (type I, Ia, II, IIa). Although the adopted channel shape in model B1b is conical with the vertex located at the origin, the field-lines clearly have a “type I conical” shape, i.e., their projection crosses the $r = 0$ axis at $z_0 < 0$ with $dz_0/d\Psi > 0$, see the right panel of Fig. 1 and Fig. 4.

Equation (B8) fits well the curves seen in Fig. 5. In one decade or so in cylindrical distance, downstream from the transition radius r_{tr} , the bunching function drops from \mathcal{S}_{tr} to $\mathcal{S}_{\text{tr}} + \Delta\mathcal{S}$. The difference $\Delta\mathcal{S} (< 0)$ corresponds to difference $\Delta\mathcal{V} \approx 2\Delta\mathcal{S}$ in the potential energy, and thus to acceleration $\Delta\Gamma = -2\Delta\mathcal{S}/mc^2$.

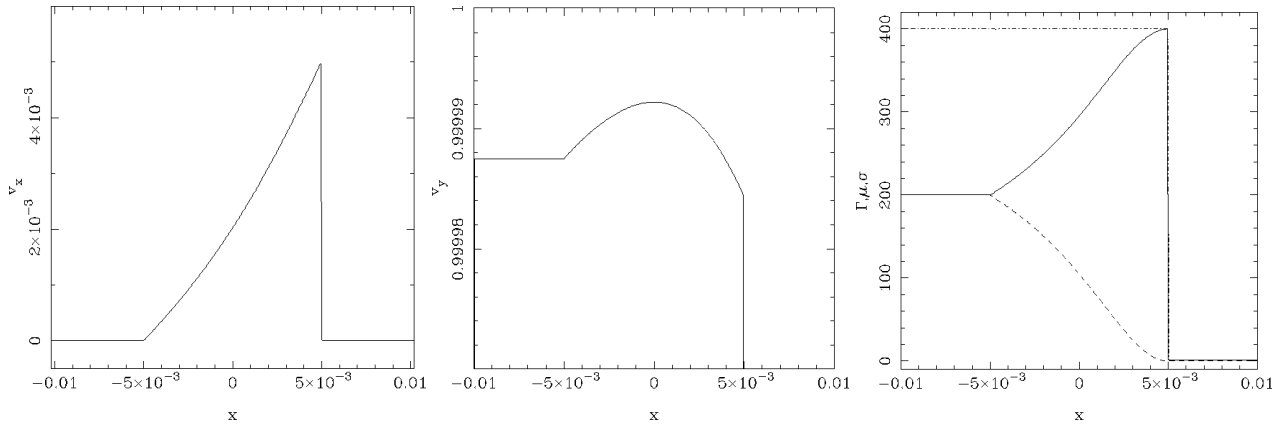


Figure A1. The one-dimensional rarefaction wave solution for the second Riemann problem described in Section 3. The solution is shown time $t = 1$ after the decay of the initial discontinuity (the dimensionless speed of light is unity). The lines in the third panel show the variation of Γ (solid line), σ (dashed) line, and μ (dash-dotted line).